Seventh International Symp. on Magnetic Bearings, August 23-25 , 2000, ETH Zurich

FAULT TOLERANCE OF A LORENTZ-TYPE SLOTLESS, SELF-BEARING MOTOR ACCORDING TO THE COILING SCHEMES

Daegon Kim
Bearing and Sealing Lab, University of Kentucky, Lexington, KY, USA, dgkim0@engr.uky.edu
Lyndon S. Stephens
Bearing and Sealing Lab, University of Kentucky, Lexington, KY, USA, stephens@engr.uky.edu

ABSTRACT
Permanent magnet (PM) self-bearing motors provide independent bearing and motor functionality in a single magnetic actuator. Typical designs have used slotted stators and thin surface mounted PM's in order to provide a minimum reluctance path for the bearing control flux such that adequate bearing forces are generated. Such designs necessarily result in smaller torque production due to the thin PM's and have large torque ripple due to the slotted stator. This paper introduces the principles of motoring torque and bearing force of the slotless thick PM's self-bearing motor and the proposes a new coil winding method to minimize the effect of coil failure without any redundant devices. Comparisons of the stiffness and stability characteristics between typical and proposed coil winding methods are presented. The analysis indicates that the proposed coil winding method can minimize the coil failure effects and the motor can levitate and rotate stably in spite of the coil failure.

INTRODUCTION
Self-bearing motors (also termed integrated motor bearings and bearingless motors) combine magnetic bearing and motoring functionality into a single magnetic actuator to perform both radial force and torque production. Such designs reduce the overall length of a motor because no mechanical bearings are required. This effectively increases power density, reduces weight and reduces the susceptibility to rotordynamic vibrations in many applications. PM self-bearing motors have been studied by Bischel [1], Chiba [2], Schoeb [3], and Okada [4], among others for a variety of applications. One commonality of these designs is that attractive forces between the rotor and stator (Maxwell-type forces) provide the bearing function, and magnetic forces on current carrying conductors (Lorentz-type forces) produce the motoring torque. As a consequence, an inherent trade-off between motoring torque and bearing force exists for these designs as thicker PMs lead to larger torque but increase the path reluctance for the bearing flux leading to smaller bearing forces. In order to optimize this trade-off and produce sufficient torque and bearing force, the stators of these designs have slots that provide a minimum reluctance flux path. A disadvantage of these slotted designs as discussed in [5], is the significant detent torque and cogging torque that is produced between the stator teeth and the rotor PM's. This is especially problematic in fine pointing and tracking applications. This paper focuses on a slotless self-bearing motor that uses the Lorentz type force to produce both the motoring torque and the bearing forces. A derivation of the linearized system equations of Maxwell type destabilizing forces due to PM's and winding flux as well as Lorentz type force is also presented. For producing both motoring torque and bearing forces and reducing cogging torque without any additional coiling and or redundant devices, many winding stations are needed, and fault tolerance to coil failure is, therefore, an important issues in the design for system reliability.

Fault tolerant operation of electromagnetic devices in the face of multiple coil and or amplifier failures is most commonly accomplished by large number of redundant devices. Most of the fault tolerant systems have focused on the amplifiers and or sensors. Further, several schemes have recently been proposed for achieving reliable electromagnetic devices including controller board approaches that make use of re-bias linearization when coil failure occurs [6][7]. Fault tolerance to coils can be achieved by an increased number of poles and coils in the actuator, and the redundant devices will be needed. These redundant devices may lead to a weight and cost debit. Therefore, this paper introduces the principles of motoring torque and bearing force of the slotless thick PM self-bearing motor and proposes a new coil winding method to minimize the effect of coil failure without any redundant devices.

ANALYSIS
Figure 1 shows the layout of the actuator consisting of M=8 PM pole pairs attached to the rotor and N_{seg}=4 individually controlled winding segments attached to the stator. Each winding segment in the motor is an arc of $\pi/2$ radians and is attached to the slotless back iron. The

windings occupy N_s stations along each winding segment ID with N_w individual wires per station. The control force and torque generation principle is straightforward for this design. Each segment generates a traction on the surface of the rotor due to the PM flux linking with the segment windings (a Lorentz-type force). By precise construction of the motor, the tractions due to segments 1-4 are resolved into the forces $F_{x,B,1}$, $F_{y,B,2}$, $F_{x,B,3}$ and $F_{y,B,4}$. By proper selection of the control currents in each segment, the segment forces are modulated to produce independent bearing forces and motoring torque.

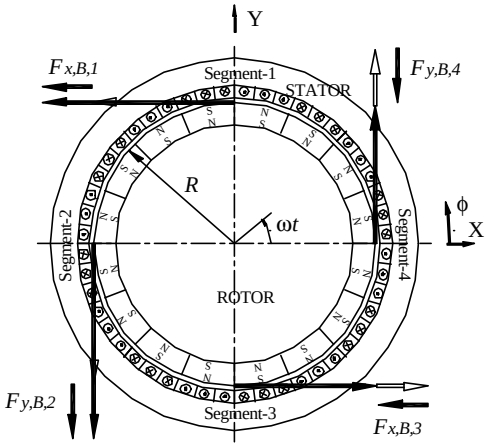

FIGURE 1: Actuator Layout and Force Generation

Air Gap Flux and Winding Current Distributions

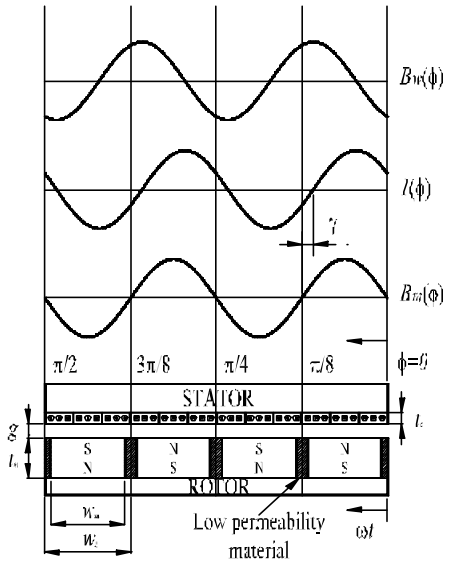

FIGURE 2: Air gap flux and current distributions for one segment

Figure 2 shows a single segment of the actuator unrolled as an approximation to the true arc geometry. Such an approximation is used for the permeance model [8] and is valid to the extent that the rotor radius R is large. The PMs of average arc length, w_m, and radial thickness, t_m, are attached to the rotor and separated by a low permeability material. The windings have radial thickness, t_c, and are separated from the PMs by the nominal radial air gap, g_0. Also shown in Figure 2 is the ideal air gap flux due to the PM's, the ideal air gap flux due to the windings and the ideal current distribution. The ideal air gap flux distribution due to the PMs in each segment is:

$$B_m(f) = \overline{B_m(f)} \sin\left[M(f - wt)\right] \tag{1}$$

where $\overline{B_m(f)}$ is the maximum flux density crossing the air gap for the rotor in an eccentric position, and calculated by:

$$\overline{B_m(f)} = \frac{w_g t_m B_r}{w_g t_m + m_R w_m k_{ml}\left[t_c + g_0 - x\cos f - y\sin f\right]} \tag{2}$$

where k_{ml} is the derating factor for magnet-to-magnet leakage and is computed as:

$$k_{ml} = 1 + \frac{4t_m}{p m_R w_m} \ln\left[1 + p\,\frac{g_0 + t_c}{w_g - w_m}\right] \tag{3}$$

The distribution of the winding current in each segment is identical with respect to the angular coordinate but is different in magnitude. The windings of the motor are approximated as a current sheet with the current distribution in the k^{th} segment approximated by:

$$I_k(f) = \frac{1}{2p} N_{seg} N_s N_w i_k \sin\left[M(f - wt + g)\right] \tag{4}$$

where i_k is the maximum current in the k^{th} segment and γ is the phase angle of the current with respect to the PM flux. Finally, the air gap flux due to the winding currents is computed using the effective permeance of the winding region, air gap and the PMs as seen by the winding flux. This expression is :

$$B_w(f) = \frac{m_0 N_{seg} N_s N_w i_k \sin\left[M(f - wt + g + p/2M)\right]}{2p\left(t_m + t_c + g_0 - x\cos f - y\sin f\right)} \tag{5}$$

where $\pi/2M$ is the phase shift of the winding flux with respect to the winding current.

Lorenz Type Bearing Forces and Torque

Given the air gap flux and winding distributions in the previous section, several different types of forces act on the rotor. Those used for bearing force and torque controls are the Lorentz-type resulting from the PM flux linking with the winding currents. Referring to Figure 1, the Lorentz-type forces are computed by:

$$\mathbf{F}_{q,B}(f) = L\sum_{k=1}^{N_{seg}}\sum_{j=1}^{N_s}\int_{f_{j-1}}^{f_j} B_m(f)\, I_k(f) \begin{Bmatrix} -\sin(f) \\ \cos(f) \end{Bmatrix} df \tag{6}$$

where $F_{q,B}(\phi)$ is expressed as $\{F_{x,B}(\phi)\ F_{y,B}(\phi)\}^T$ and L is the axial length of the actuator. Flux and current distributions are given by eq (1) and (4). The integration limits ϕ_{j-1} and ϕ_j of the k^{th} segment and j^{th} winding station in eq (6) can be presented as functions of k and j as $\phi_{j-1}=(j-1)\pi/(2N_s)+(2k-1)\pi/4$ and $\phi_j=j\pi/(2N_s)+(2k-1)\pi/4$. Similarly, the total torque produced by the actuator is computed using:

$$T(f)=RL\sum_{k=1}^{N_{seg}}\sum_{j=1}^{N_s}\int_{f_{j-1}}^{f_j} B_m(f)I_k(f)df \qquad (7)$$

where $T(\phi)$ is the total actuator torque, and R is the outside radius of the rotor. Control of the actuator such that independent torque and force generation is achieved, depends upon proper selection of the segment winding currents. In the real system $F_{q,B}(\phi)$ and $T(\phi)$ vary with angular position of the rotor ωt. This selection must be done with respect to three control currents, i_x, i_y and i_θ that correspond to the forces and torque in each direction. The system is over-determined in that a total of four segment forces are being used to generate two control forces and one torque. Therefore, there are many different current relationships to choose from, but the simplest is:

$$\begin{aligned} i_1 &= i_q - i_x \\ i_2 &= i_q - i_y \\ i_3 &= i_q + i_x \\ i_4 &= i_q + i_y \end{aligned} \qquad (8)$$

The magnitude of the Lorentz type forces and torque depend upon the displacement of the rotor x and y, and the control current i_x and i_y. These forces and torque are linearized using Taylor series expansion at $x=y=i_x=i_y=0$. The actuator has many winding stations resulting in smooth torque and bearing force generation, therefore it is assumed that the forces generated by the k^{th} segment and j^{th} winding station are concentrated at a mid-point of those winding stations. The equation (6) is approximated as:

$$\mathbf{F}_{q,B}=\mathbf{F}_{0,B}+\mathbf{K}_{q,B}\mathbf{q}+\mathbf{K}_{i,B}\mathbf{i}+\cancel{H.O.T}^{\approx 0} \qquad (9)$$

where in eq (9) the high order terms are neglected. **Q** is $\{x\ y\}^T$, **i** is $\{i_x\ i_y\}^T$, and $\mathbf{F}_{0,B}$ is the Lorentz type destabilizing force matrix and calculated by:

$$\mathbf{F}_{0,B}=\overline{K_{i,B}}i_q\sum_{k=1}^{N_{seg}}\sum_{j=1}^{N_s}\Lambda_B\begin{Bmatrix}-\sin(f_{kjm})\\ \cos(f_{kjm})\end{Bmatrix} \qquad (10)$$

In the no fault case the destabilizing forces $F_{0x,B}$ and $F_{0y,B}$ are zero due to symmetry. $\mathbf{K}_{q,B}$ in eq (12) is the displacement stiffness coefficient matrix of the Lorentz type force and calculated by:

$$\mathbf{K}_{q,B}=\overline{K_{q,B}}\sum_{k=1}^{N_{seg}}\sum_{j=1}^{N_s}\Lambda_B\begin{bmatrix}-\sin(f_{kjm})\cos(f_{kjm}) & \sin^2(f_{kjm})\\ \cos^2(f_{kjm}) & \sin(f_{kjm})\cos(f_{kjm})\end{bmatrix} \qquad (11)$$

In the no fault case the diagonal elements $K_{xx,B}$ and $K_{yy,B}$ are zero and the cross-coupled elements $K_{xy,B}$ and $K_{yx,B}$ are non-zero. $\mathbf{K}_{i,B}$ is the current stiffness coefficient matrix of the Lorentz type force and calculated by:

$$\mathbf{K}_{i,B}=\overline{K_{i,B}}\sum_{j=1}^{N_s}\Lambda_B\begin{bmatrix}\sin(f_{1jm})-\sin(f_{3jm}) & \sin(f_{2jm})-\sin(f_{4jm})\\ -\cos(f_{1jm})+\cos(f_{3jm}) & -\cos(f_{2jm})+\cos(f_{4jm})\end{bmatrix} \qquad (12)$$

In the no fault case the cross-coupled elements $K_{ixy,B}$ and $K_{iyx,B}$ are zero but the diagonal elements $K_{ixx,B}$ and $K_{iyy,B}$ are not zero. Similarly, the torque equation (7) simplifies to:

$$T=T_0+K_{qx}x+K_{qy}y \qquad (13)$$

where T_0 is the nominal motor torque generated by Lorentz forces and calculated by:

$$T_0=Ri_q\overline{K_{i,B}}\sum_{k=1}^{N_{seg}}\sum_{j=1}^{N_s}\Lambda_B \qquad (14)$$

$K_{\theta x}$ and $K_{\theta y}$ in eq (13) are open loop torsional stiffness coefficients and expressed by:

$$\begin{aligned} K_{qx} &= R\overline{K_{q,B}}\sum_{k=1}^{N_{seg}}\sum_{j=1}^{N_s}\Lambda_B\cos(f_{kjm}) \\ K_{qy} &= R\overline{K_{q,B}}\sum_{k=1}^{N_{seg}}\sum_{j=1}^{N_s}\Lambda_B\sin(f_{kjm}) \end{aligned} \qquad (15)$$

In the no fault case the open loop torsional stiffness coefficients $K_{\theta x}$ and $K_{\theta y}$ are zero due to symmetry. The other constant terms are calculated using:

$$\overline{K_{i,B}}=\frac{w_g t_m LN_{seg}N_s N_w B_r}{2p\left[w_g t_m+m_R w_m k_{ml}(t_c+g_0)\right]} \qquad (16)$$

$$\overline{K_{q,B}}=\frac{m_R w_g w_m t_m k_{ml} LN_{seg}N_s N_w B_r i_q}{2p\left[w_g t_m+m_R w_m k_{ml}(t_c+g_0)\right]^2} \qquad (17)$$

$$\begin{aligned}\Lambda_B=\frac{\cos(Mg)}{2}(f_j-f_{j-1})-\frac{1}{4M}\big[&\sin(2Mf_j-2Mwt+Mg)\\ &-\sin(2Mf_{j-1}-2Mwt+Mg)\big]\end{aligned} \qquad (18)$$

Maxwell Type Destabilizing Forces due to PM

Now examine the sensitivity of the Maxwell type forces due to PM to small rotor displacements. The Maxwell type forces are dependent only upon the square of the air gap flux due to the PM's, but are not dependent upon the current distribution of the winding station. The attractive forces between the rotor and stator generated at i^{th} PM region are given by:

$$\mathbf{F}_{q,M}(f)=\frac{RL}{2m_0}\sum_{i=1}^{2M}\int_{f_{i-1}}^{f_i}B_m^{\,2}(f)\begin{Bmatrix}\cos(f)\\ \sin(f)\end{Bmatrix}df \qquad (19)$$

where $\mathbf{F}_{q,M}(\phi)$ is the Maxwell type force matrix due to the PM's and expressed by $\{F_{x,M}(\phi)\ F_{y,M}(\phi)\}^T$. Similar to the analysis of the Lorentz force, $\mathbf{F}_{q,M}$ is also linearized using Taylor series expansion at x=y=0. Because there are many PM poles in the rotor, it is assumed that the force generated by the i^{th} magnet section is concentrated at a mid-point of that magnet section, and expressed as $\phi_{im}=(i-1/2)\pi/M+\omega t$. Equation (19) is approximated as:

$$\mathbf{F}_{q,M}=\mathbf{K}_{q,M}\mathbf{q}+\cancelto{\approx 0}{H.O.T} \qquad (20)$$

where in eq (20) the high order terms are neglected. $\mathbf{K}_{q,M}$ is the displacement stiffness coefficient matrix of the Maxwell type forces due to PM's and where the only diagonal components are non-zero and is expressed by:

$$K_{xx,M}=K_{yy,M}=\frac{pm_R w_m k_{ml} RLt_m^{\,2} w_g^{\,2} B_r^{\,2}}{2m_0\left[w_g t_m+m_R w_m k_{ml}(t_c+g_0)\right]^3} \qquad (21)$$

where $K_{xx,M}$ and $K_{yx,M}$ are diagonal elements and also independent of ωt. By examining the symmetry of the PM flux within the actuator, one can clearly see that the cross-coupled displacement stiffness terms should be zero and the direct terms should not.

Maxwell Type Destabilizing Forces due to Winding Flux

Finally, the destabilizing side pull forces on the rotor due to the winding flux are considered. In this case, side pull forces result even when the rotor is in the centered position. Maxwell forces due to winding currents depend on the square of the winding flux expressed in eq (5) and are given by:

$$\mathbf{F}_{q,W}(f)=\frac{RL}{2m_0}\sum_{k=1}^{N_{seq}}\sum_{j=1}^{N_s}\int_{f_{j-1}}^{f_j}B_w(f)^2\begin{Bmatrix}\cos(f)\\ \sin(f)\end{Bmatrix}df \qquad (22)$$

In the same way it is assumed that the forces generated at any winding stations are concentrated the station's mid-point, and linearized using a Taylor series expansion at $x=y=i_x=i_y=0$. Eq (22) simplified as:

$$\mathbf{F}_{q,W}=\mathbf{F}_{0,W}+\mathbf{K}_{q,W}\mathbf{q}+\mathbf{K}_{i,W}\mathbf{i}+\cancelto{\approx 0}{H.O.T} \qquad (23)$$

In the same way the high order terms are neglected, and $\mathbf{F}_{q,W}$ is expressed as $\{F_{x,W}(\phi)\ F_{y,W}(\phi)\}^T$, $\mathbf{F}_{0,W}$ is the Maxwell type destabilizing force matrix due to winding flux, $\mathbf{K}_{q,W}$ and $\mathbf{K}_{i,W}$ are the displacement and current stiffness coefficients matrix, and expressed by:

$$\mathbf{F}_{0,W}=\frac{\overline{K_{i,W}i_q}}{2}\sum_{k=1}^{N_{seq}}\sum_{j=1}^{N_s}\Lambda_W\begin{Bmatrix}\cos(f_{kjm})\\ \sin(f_{kjm})\end{Bmatrix} \qquad (24)$$

$$\mathbf{K}_{q,W}=\overline{K_{q,W}}\sum_{k=1}^{4}\sum_{j=1}^{N_s}\Lambda_W\begin{bmatrix}\cos^2(f_{kjm}) & \cos(f_{kjm})\sin(f_{kjm})\\ \cos(f_{kjm})\sin(f_{kjm}) & \sin^2(f_{kjm})\end{bmatrix} \qquad (25)$$

$$\mathbf{K}_{i,W}=\overline{K_{i,W}}\sum_{j=1}^{N_s}\Lambda_W\begin{bmatrix}-\cos(f_{1jm})+\cos(f_{3jm}) & -\cos(f_{2jm})+\cos(f_{4jm})\\ -\sin(f_{1jm})+\sin(f_{3jm}) & -\sin(f_{2jm})+\sin(f_{4jm})\end{bmatrix} \qquad (26)$$

In the no fault case the static force matrix elements $F_{0x,W}$ and $F_{0y,W}$, the cross-coupled elements of the displacement stiffness coefficient matrix eq (25), $K_{xx,W}$ and $K_{yy,W}$,and the diagonal elements in the current stiffness coefficient matrix eq (26) are zero. The other constant terms are calculated by:

$$\overline{K_{q,W}}=\frac{m_0 RLN_{seg}^{\,2}N_s^{\,2}N_w^{\,2}i_q^{\,2}}{p^2M^2(t_m+t_c+g_0)^3} \qquad (27)$$

$$\overline{K_{i,W}}=\frac{4m_0 RLN_{seg}^{\,2}N_s^{\,2}N_w^{\,2}i_q}{p^2M^2(t_m+t_c+g_0)^2} \qquad (28)$$

$$\Lambda_W=\frac{f_j-f_{j-1}}{2}-\frac{1}{4M}[\sin(2Mf_j-2Mwt+Mg)-\sin(2Mf_{j-1}-2Mwt+Mg)] \qquad (29)$$

Dynamic System Equations and Feedback Control

The equivalent forces can be written in terms of the Lorentz type bearing control forces, $F_{x,B}$, $F_{y,B}$, the Maxwell type forces due to PM's, $F_{x,M}$, $F_{y,M}$, and the Maxwell type forces due to winding flux, $F_{x,W}$, $F_{y,W}$. In the previous section all these forces were linearized and expressed by the displacement and current stiffness coefficient. Therefore the dynamic system equation is as:

$$\mathbf{M}\ddot{\mathbf{q}}-\mathbf{K}_q\mathbf{q}=\mathbf{F}_0+\mathbf{K}_i\mathbf{i} \qquad (30)$$

where $\mathbf{M}$ is mass matrix, $\mathbf{K}_q$ is the displacement stiffness coefficient matrix, $\mathbf{K}_i$ is the current stiffness coefficient matrix, and $\mathbf{F}_0$ is the destabilizing force matrix. Each matrix can be calculated by:

$$\mathbf{F}_0=\mathbf{F}_{0,B}+\mathbf{F}_{0,W} \qquad (31)$$

$$\mathbf{K}_q=\mathbf{K}_{q,B}+\mathbf{K}_{q\,M}+\mathbf{K}_{q,W} \qquad (32)$$

$$\mathbf{K}_i=\mathbf{K}_{i,B}+\mathbf{K}_{i,W} \qquad (33)$$

Figure 3 shows the feedback control for the actuator. The sensor measurements are used to construct error signals, which are fed into PID controllers. The control signals, V_x, V_y and V_θ are combined using a set of summing and differencing junctions to produce each segment control signal V_1, V_2, V_3 and V_4. The sinusoidal current sheet of eq (4) is approximated by 12 phases (3 per segment) that are constructed using cosine functions that are 60 degrees out of phase with one another and by using a special winding scheme.

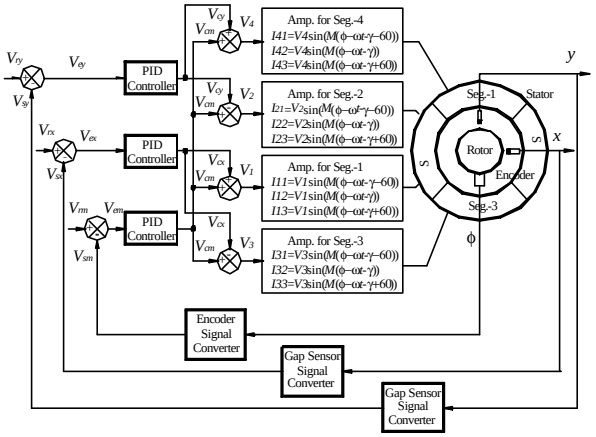

FIGURE 3: Self-bearing motor feedback control

Coiling Method

Figure 4 shows 3 different coil winding methods for a segment, where the number of winding stations are 12 and the 3 phase currents φ_1, φ_2, and φ_3 are considered. The arrows indicate the current flow direction and each phase is shifted by 60 degrees. Figure 4 (a) is wound serially which is the typical used winding method, (b) is wound paralelly with unsymmetry and (c) is wound paralelly with symmetry.

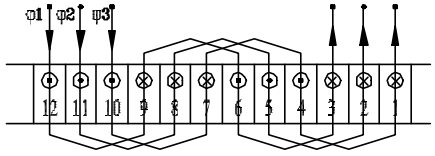

(a) Serial Winding

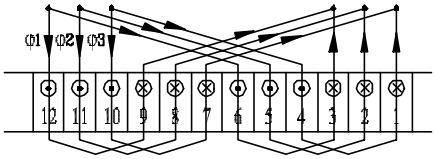

(b) Unsymmetric Parallel Winding

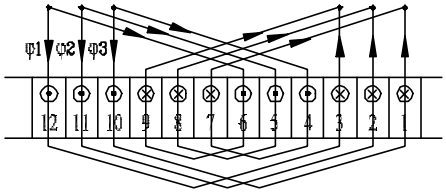

(c) Symmetric Parallel Winding

FIGURE 4: Coil winding

SIMULATION RESULTS

In the previous section the traditional serial winding method and two kinds of new winding method were presented. In the no fault case the dynamics of the rotor under closed loop control are the same. However, when the coil in any winding station is open, the system dynamics are quite different. As an example of fault tolerance of the winding station, let's consider a coil in the number 11 winding station is open due to any physical problem. In the typical winding case (a) the forces cannot be generated at the winding station 11, 8, 5 and 2, in the case (b) at winding station 11 and 8, and in the case (c) at the winding station 11 and 2. A prototype self-bearing motor with the properties listed in Table 1 is under construction. These properties are used in a simulation of the stability and the motor response to a rotating unbalance at constant angular velocity of 955 RPM.

TABLE 1: Summary of prototype motor construction

Property	Sym	Value
No. of PM Pole Pairs	M	8
No. of Segments	N_{seg}	4
No. of Winding Stations per Seg	N_s	12
No. of Wires per Winding Station	N_w	85
Remnance Flux	B_r(T)	1.01
Radial Thickness of PM's	t_m(mm)	7.75
Radial Thickness of coil windings	t_c(mm)	3.87
Nominal radial air gap	g_o(mm)	0.76
Rotor Outer Radius	R(mm)	50.8
Motor Length	L(mm)	25.4

TABLE 2: Comparison of motor properties for γ=0

Property	No fault case	Serial	Unsym. parallel	Sym. parallel
T (Nm)	6.25	5.3	5.78	5.78
F_{0x} (N)	0	17	8.6	7.7
F_{0y} (N)	0	-1	1.2	-0.48
K_{xx} (N/m)	62188	62156	62035	62159
K_{xy} (N/m)	6658	4982	5833	5957
K_{yx} (N/m)	6658	6307	6495	6345
K_{yy} (N/m)	62188	62032	62247	62123
K_{ixx} (N/A)	14	9.6	11.7	12
K_{ixy} (N/A)	1.7	1.7	1.7	1.7
K_{iyx} (N/A)	1.7	-1.2	-1.9	-1.5
K_{iyy} (N/A)	14	13.9	13.9	14

TABLE 3: Comparison of motor properties for γ=0.01

Property	No fault case	Serial	Unsym. parallel	Sym. parallel
T (Nm)	6.24	5.2	5.76	5.76
F_{0x} (N)	0	16.9	8.5	7.8
F_{0y} (N)	0	0	1.7	0
K_{xx} (N/m)	61723	61715	61582	61716
K_{xy} (N/m)	6637	4966	5805	5939
K_{yx} (N/m)	6637	6287	6465	6325
K_{yy} (N/m)	61723	61684	61840	61707
K_{ixx} (N/A)	13.9	9.6	11.7	11.9
K_{ixy} (N/A)	0.5	0.5	0.5	0.5
K_{iyx} (N/A)	- 0.5	-0.4	-0.9	-0.4
K_{iyy} (N/A)	13.9	13.9	13.9	13.9

Table 2 summarizes the comparison of the stiffness coefficient and other properties for a phase angle γ=0. The simulated results indicate that the torque of the proposed parallel winding methods are better than the traditional

serial winding method compared with no fault case. The destabilizing forces F_{0x} and F_{0y} are generated at the fault case, in which the destabilizing forces are minimum at the symmetric parallel winding. Among the stiffness coefficients the diagonal current stiffness coefficients K_{ixx} and K_{iyy} are important parameters in the system, because the system is controlled by these. Table 2 indicates that the proposed symmetric parallel winding under a fault condition out performs the other two winding methods. Similarly, Table 3 summarizes the comparison of the stiffness coefficient and other properties for a phse angle γ=0.01. The torque is slightly smaller as compared with the case of the phase angle γ=0. Again, the symmetric parallel winding method is better than the other winding methods in spite of none zero phase angle.

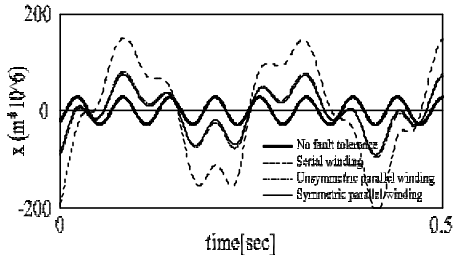

(a) X-directional displacement

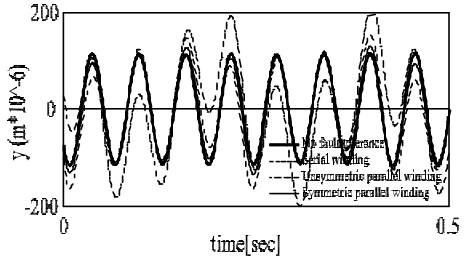

(b) Y-directional displacement

FIGURE 5: Comparison of the displacement for γ=0

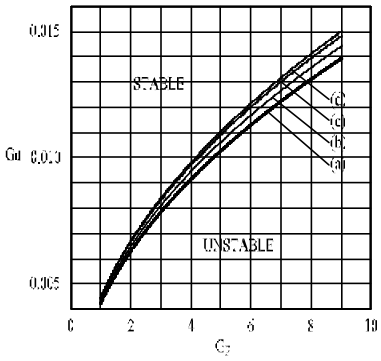

FIGURE 6: Stability criterion for γ=0: (a) No fault, (b) Serial winding, (c) Unsymmetric parallel winding, (d) Symmetric parallel winding

Figure 5 shows the comparison of the simulated displacement of the rotor for a phase angle γ=0. The simulation results in figure 5a indicate that the x-directional displacements of the proposed unsymmetric and symmetric winding method are very similar and better than the typical serial winding method, however, the response of the symmetric winding case is better than unsymmetric winding case comparing y-directional displacement in Figure 5b. Figure 6 shows the comparison of the stability criterion for γ=0 and the integral control gain G_i=0, where the saturation and nonlinear effects were not considered in this analysis. In this analysis Hurwitz stability criterion was used. If we select the proportional and derivative gains, G_{ip} and G_{id}, at the upper region of the curve, the system will work stably. In the fault case the stable region corresponding to the symmetric winding method is better than other winding methods.

CONCLUSION

This paper showed the principles of motoring torque and bearing force of the slotless thick PM's self-bearing motor. Lorentz type forces and Maxwell type forces due to PM's and winding flux were linearized, and a set of simplified system dynamic equations was derived. This paper also proposed a new coil winding method to minimize the effect of coil failure without any redundant devices. Analysis showed that the proposed symmetric parallel coil winding method has better performance than typical serial coil winding method whether the phase angle γ=0 or not.

REFERENCE

1. J. Bischel, "The Bearingless Electrical Machine," in *Proc. Int. Symp Magn. Suspension Technol.'91*, NASA Publication 3152, Langley Research Center, Hampton, VA, pp. 561-573, August, 1991.
2. A. Chiba, M.A. Rahman, and T. Fukao, "Radial Forces in Bearingless Reluctance Motor," *IEEE Trans. Magnetics*, vol. 27, p. 786, Mar. 1991.
3. R. Schoeb and J. Bichel, "Vector Control of Bearingless Motor," in *Proc. 4th Int. Symp. Magn. Bearings*, ETH Zurich, Switzerland, pp. 327-332, 1994.
4. Y. Okada, S. Miyamoto, and T. Ohishi, "Levitation and Torque Control of Internal PM type Bearingless motor," *IEEE Trans. Control Syst. Techn.*, vol. 4, no. 5, pp. 565-571, 1996.
5. M.A. Casemore and L.S. Stephens, "Actuator Gains for a Toothless Permanent-Magnet Self-Bearing Motor", *IEEE Trans. on Magnetics*, vol. 35, No. 6, November, 1999.
6. Dominick Montie, "Self-Sensing in Fault Tolerant Magnetic Bearings," in *Trans. of the ASME, 99-GT-178*, Jun. 1999.
7. D. C. Meeker, "Optimal solutions to the Inverse Problem in Quadratic Magnetic Actuators," ROMAC Report no. 392, May 1996.
8. L. S. Stephens and Daegon Kim "Analysis and Simulation of a Lorentz-type Slotless, Self-Bearing Motor," *Proc. Of 1st IFAC Conf. On Mechatronic System*, Sep. 2000.